Investigation of Ion Beam Extraction Mechanism for Higher Thrust Density of Ion Thrusters

IEPC-2015-453p／ISTS-2015-b-453p

Presented at Joint Conference of 30th International Symposium on Space Technology and Science 34th International Electric Propulsion Conference and 6th Nano-satellite Symposium, Hyogo-Kobe, Japan July 4 – 10, 2015

Kenta Hiramoto[1]
Yokohama National University, Yokohama, 240-8501, Japan

Abstract: We have investigated ion beam extraction mechanism using two dimensional axisymmetric particle-in-cell simulations with Monte Carlo collisions (PIC/MCC) under various conditions, such as beam voltage, absorbed power, and grid structures. The plasma region, which is enclosed by a 1-mm-thick dielectric cylinder with a five-turn coil, is 5.0 mm in radius and 10 mm in length. The PIC/MCC results have shown that more absorbed power is required to extract more ions from the plasma source, and that the ion beam current is not affected by the diameter of the screen grid hole. In addition, we have obtained that the optimum value of the difference between the diameter of the screen grid hole and that of the accelerator grid hole is 1.4 mm under the following conditions: the absorbed power is 500 mW, the beam voltage is 1100 V, and the thickness of the screen grid is 0.3 mm.

Nomenclature

m	=	mass
q	=	charge
$\mathbf{B}$	=	magnetic field
$\mathbf{E}$	=	electric field
v	=	velocity
x	=	position.
n	=	number density
ρ	=	charge density
ε_0	=	vacuum permittivity
μ_0	=	vacuum permeability
k_B	=	Boltzmann's constant
T_e	=	electron temperature
I	=	current
i	=	current density
V_0	=	potential difference between the screen and the accelerator grids
P_{abs}	=	absorbed power
l	=	gap distance between the screen and the accelerator grids
t_{sc}	=	thickness of the screen grid
t_{ac}	=	thickness of the accelerator grid
d_{sc}	=	hole diameter of the screen grid
d_{ac}	=	hole diameter of the accelerator grid

[1] Graduate student, Department of Systems Integration, 79-5 Tokiwadai, Hodogaya-ku, Yokohama, Japan.
E-mail: hiramoto-kenta-tm@ynu.jp

I. Introduction

RECENTLY, miniaturization of satellites has been very popular. It makes possible to decrease mission costs and development period, and thus even small companies and universities can launch and operate microsatellites. However, microsatellites have limits of weight, volume, and power, which requires that thrusters mounted on them must be small.[1] One of such thrusters can be ion thrusters. A 50 kg-class satellite, HODOYOSHI-4, was developed by the University of Tokyo and the Next Generation Space Technology Research Association (NESTRA) in Japan, and launched in 2014. The satellite mounted a miniature ion propulsion system (MIPS), [2] and the MIPS was already operated in space.

Ion thrusters have high specific impulse and efficiency, while the thrust density is very low, which requires long-term operation for acceleration. If ion thrusters provided higher thrust density, their applications would be expanded. NASA GRC already started working on the development of high-thrust density ion engines for high power applications in collaboration with The Aerospace Corporation, and the University of Michigan.[3,4] Although they focus on the application to high-power primary propulsion, the technology would also be applicable to micropropulsion. In our early studies, we developed a two-dimensional particle model for a micro RF ion thruster and investigated the plasma parameters and ion beam profiles.[5] In this model, the plasma generation and the ion beam acceleration can be analyzed simultaneously. Since the ion beam extraction is dependent on the characteristics of the plasma source as well as the grid structure, it is better to analyse the plasma generation and the ion beam acceleration continuously. In this study ion beam extraction mechanism has been investigated using this particle model to find the best condition of the beam extraction for higher thrust density.

II. Numerical Model

A. Configuration

In this analysis, we have conducted two-dimensional particle-in-cell simulations with Monte Carlo collisions (PIC/MCC). Figure 1 shows our calculation model. The plasma region, which is enclosed by a 1-mm-thick dielectric cylinder with a five-turn coil, is 5.0 mm in radius and 10 mm in length. The ion accelerator system consists of screen and accelerator grids, and the vacuum region, where ion beam is extracted, is 6.0 mm in radius and 20 mm in length. In addition, a ground electrode is positioned 1 mm downstream of accelerator grid. Since the calculation is carried out for both the plasma region and the vacuum region, no assumptions are required for the ion beam extraction.

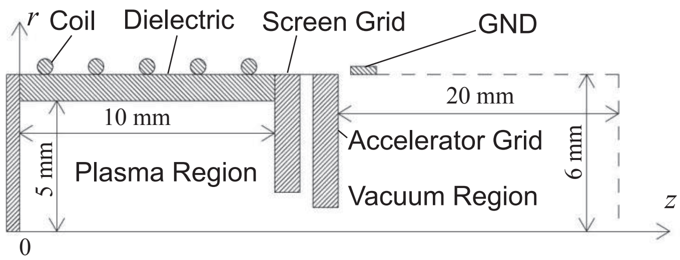

Figure 1. Calculation model

B. Assumption

We have investigated under the following assumptions.

i). Only electron and singly-ionized Xe^+ are treated as particles.

ii). Neutral particles are spatially and temporally uniform with a Maxwellian distribution at a gas temperature of 300 K in the plasma region. Additionally, there are no collisions downstream of accelerator.

iii). The reactions between charge and neutrals are elastic, excitation, and ionization collision for electrons[6-8], and elastic and charge exchange collisions for ions.[9]

$e + Xe \rightarrow e + Xe$ (Elastic collision).

$e + Xe \rightarrow e + Xe^*$ (Excitation).

$e + Xe \rightarrow e + Xe^+ + e$ (Ionization).

$Xe^+ + Xe \rightarrow Xe^+ + Xe$ (Elastic collision).

$Xe^+ + Xe \rightarrow Xe + Xe^+$ (Charge exchange).

C. Motion and collisions of charged particles

The equation of motion for charged particles is described by

$$\frac{d\mathbf{v}}{dt} = \frac{q}{m}\left(\mathbf{E} + \mathbf{v} \times \mathbf{B}\right), \tag{1}$$

$$\frac{d\mathbf{x}}{dt} = \mathbf{v}. \tag{2}$$

Equations (1) and (2) are solved by leap-frog method and Buneman-Boris method.[10] In this study, we assume axisymmetric model, so that the position advance of particles closed to axis poses singular problems. To avoid these problems, we employ coordinate rotation.[10] We also employ the null-collision method in MCC with cross sections for electrons and ions, to reduce calculation time.[11]

D. Electrostatic field

The electrostatic field **E** and the potential ϕ are given by

$$\mathbf{E} = -\nabla\phi, \tag{3}$$

$$\left(\frac{\partial^2}{\partial r^2} + \frac{1}{r}\frac{\partial}{\partial r} + \frac{\partial^2}{\partial z^2}\right)\phi = -\frac{\rho(r,z)}{\varepsilon_0}. \tag{4}$$

Equation (4) is solved by using method of successive-over-relaxation (SOR). The boundary conditions of ϕ are zero radial potential gradient on the z axis ($\partial\phi/\partial r = 0$ at $r = 0$) due to the axisymmetry, and zero potential at all the walls. Here, to eliminate an axisymmetric error of charge density on the z axis, we employ a symmetric spline weighting by J. P. Verboncoeur.[12] In addition, to decrease a scattering of distribution for charge density, we correct by using a digital smoothing algorithm.[13]

E. Electromagnetic field

In our model, we assume that the coil is composed of five concentric rings, so that the electric field by coil has only θ–directional component. All quantities, such as electric field and current density, are also assumed harmonic oscillation depending on time. Then, θ–directional components of the electric field E_θ and the plasma current density j_θ are described as

$$E_\theta = \widetilde{E}_\theta e^{i\omega t}, \tag{5}$$

$$j_\theta = \widetilde{J}_\theta e^{i\omega t}, \tag{6}$$

where i is the imaginary unit, ω is the rf angular frequency, $\widetilde{E_\theta}$ and $\widetilde{J_\theta}$ are the complex amplitude, which satisfy the following equation:[14]

$$\left(\frac{\partial^2}{\partial r^2} + \frac{1}{r}\frac{\partial}{\partial r} + \varepsilon_0\mu_0\omega^2 - \frac{1}{r^2} + \frac{\partial^2}{\partial z^2}\right)\widetilde{E}_\theta = i\omega\mu_0\widetilde{J}_\theta. \tag{7}$$

The boundary conditions are $\widetilde{E_\theta} = 0$ at the metal walls and on the z axis ($r = 0$). The electric field on the plasma-dielectric window interfaces is analytically derived from Biot-Savart's law, and the magnetic field **B** is given by Faraday's law.

$$\nabla \times \mathbf{E} = -\frac{\partial \mathbf{B}}{\partial t}. \tag{8}$$

F. Equations for evaluation

Generally, the ion beam current is evaluated by Child-Langmuir law:

$$i_{\mathrm{CL}} = \frac{4\varepsilon_0}{9}\sqrt{\frac{2e}{m_{\mathrm{i}}}}\frac{V_0^{3/2}}{l_{\mathrm{e}}^2}, \tag{9}$$

where l_{e} is the effective gap distance of grids given by

$$l_{\mathrm{e}} = \sqrt{(l + t_{\mathrm{sc}})^2 + \frac{d_{\mathrm{sc}}^2}{4}}. \tag{10}$$

Although the Child-Langmuir law depends on only grid structure, it does not consider the plasma parameters, such as the plasma density and the electron temperature. In this study, then, we have also compared the calculated current with the ion saturation current:

$$i_{\mathrm{pi}} = qn_{\mathrm{s}}u_{\mathrm{s}} = qn_{\mathrm{p}}\sqrt{\frac{k_{\mathrm{b}}T_{\mathrm{e}}}{m_{\mathrm{i}}}}\exp\left(-\frac{1}{2}\right), \tag{11}$$

where n_{p} is a plasma density.

III. Results and Discussion

A. Dependence of potential difference

Figure 2 shows the dependence of potential difference between screen and accelerator grids, where I_{b} is the calculated current, I_{CL} is the current by Child-Langmuir law, and I_{pi} is the saturation current, and Table 1 shows the grid potentials. Other conditions are as follows: absorbed power P_{abs} = 200 mW, the gap distance between grids l = 0.5 mm, the screen grid thickness t_{sc} = 1.0 mm, the accelerator grid thickness t_{ac} = 1.0 mm, the hole diameter of the screen grid d_{sc} = 3.0 mm, and the hole diameter of the accelerator grid d_{ac} = 1.8 mm. Figure 2, shows that the increase in potential difference has little effect on the increase in calculated current. We consider that it is due to the limit of the ion saturation current for low plasma density.

Table 1. Conditions of grid potentials between the grids.

V_0 (V)	V_{sc} (V)	V_{ac} (V)
550	500	−50
880	800	−80
1100	1000	−100
1650	1500	−150

B. Dependence of absorbed power

Figures 3 and 4 show the dependence of absorbed power, where Fig. 3 is at V_0 = 1100 V and Fig. 4 is at V_0 = 1650 V. Other conditions are as follows: l = 0.5 mm, t_{sc} = 1.0 mm, t_{ac} = 1.0 mm, d_{sc} = 3.0 mm, and d_{ac} = 1.8 mm. In either case, with increasing absorbed power, the ion saturation and the calculated currents have increased. However, the calculated current is very small compared with the Child-Langmuir law and ion saturation currents at higher absorbed power. We consider that the grid electrode structure is not appropriate for higher plasma density. Here, the distributions of ion densities for P_{abs} = 100, 200, 500 mW at V_0 = 1650 V are shown in Fig. 5, and the screen grid

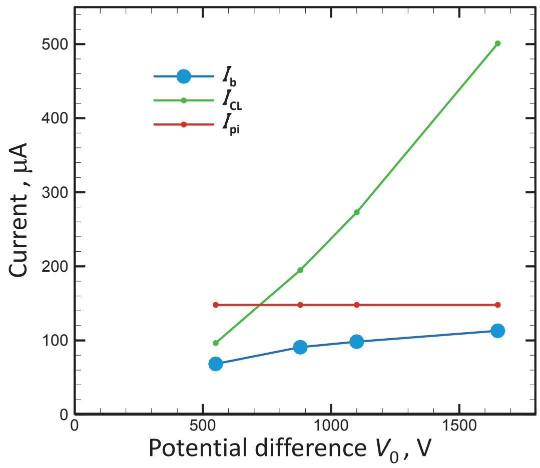

Figure 2. Dependence of potential difference between grids.

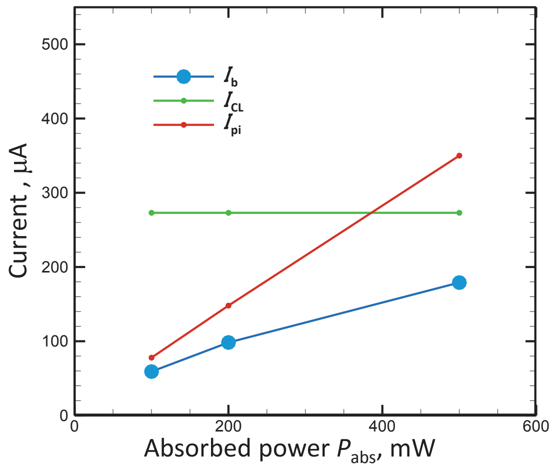

Figure 3. Dependence of absorbed power (V_0 = 1100 V).

current I_{sc} and the accelerator grid current I_{ac} are listed in Table 2. Figure 5(c) shows that some of ion beam at P_{abs} = 500 mW directly encounter the accelerator grid before focusing, so that the accelerator grid current have increased as shown in Table 2.

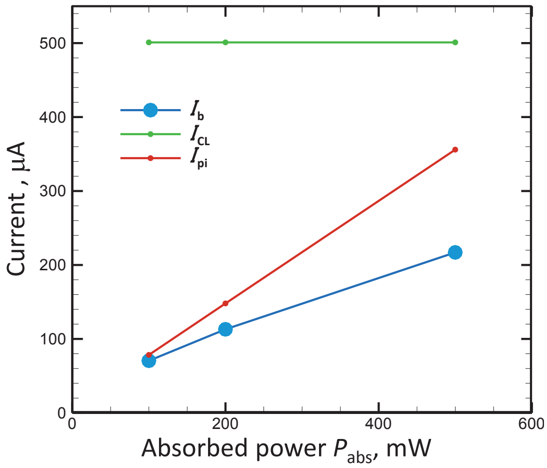

Figure 4. Dependence of absorbed power (V_0 = 1650 V).

C. Optimization of the grid structure

1. Dependence of the gap distance between grids

Figure 6 shows the dependence of the gap distance between screen and accelerator grids. Other conditions are as follows: P_{abs} = 500 mW, V_0 = 1100 V, t_{sc} = 0.3 mm, t_{ac} = 0.3 mm, d_{sc} = 3.0 mm, and d_{ac} = 1.8 mm. In this case, with increasing the gap distance, the calculated current has decreased. The gradient of the calculated current agrees with that of the Child-Langmuir law current, so that it is appropriate to include the gap distance l in the effective gap distance l_e given by Eq. (10).

2. Dependence of the grids thickness

Figure 7 shows the dependence of the screen grid thickness. Other conditions are as follows: P_{abs} = 500 mW, V_0 = 1100 V, l = 0.8 mm, t_{ac} = 0.3 mm, d_{sc} = 3.2 mm, and d_{ac} = 1.8 mm. In this case, with increasing the screen grid thickness, the calculated current have decreased, and the gradient of the calculated current agrees with that of the Child-Langmuir law current.

Figure 8 shows the dependence of the accelerator grid thickness. Other conditions are as follows: P_{abs} = 500 mW, V_0 = 1100 V, l = 0.8 mm, t_{sc} = 0.3 mm, d_{sc} = 3.2 mm, and d_{ac} = 1.8 mm. As shown in Fig. 8, it is found that the accelerator thickness does not affect the beam current.

From Figs. 7 and 8, it is reasonable to include the screen grid thickness and not to include the accelerator grid thickness in the effective gap distance l_e.

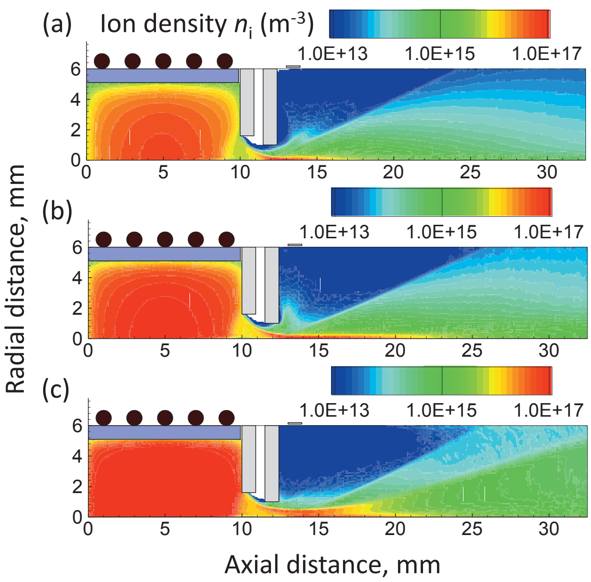

Figure 5. Ion density at V_0 = 1650 V, (a) P_{abs} = 100 mW, (b) P_{abs} = 200 mW, (c) P_{abs} = 500 mW.

Table 2. Currents for dependence of absorbed power at V_0 = 1650 V.

P_{abs} (mW)	I_b (μA)	I_{sc} (μA)	I_{ac} (μA)
100	70.5	71.2	0.72
200	113	116	2.85
500	217	225	8.64

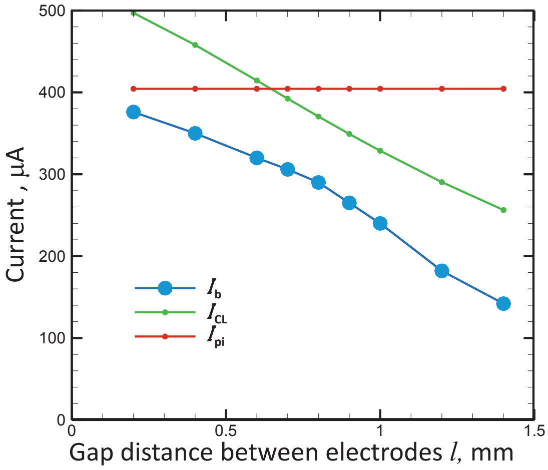

Figure 6. Dependence of the gap distance between grids.

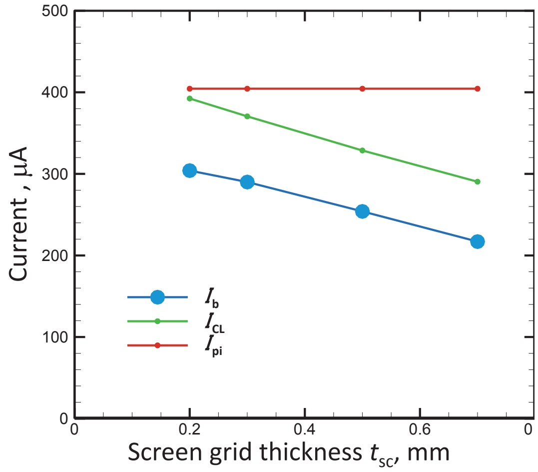

Figure 7. Dependence of the screen grid thickness.

3. Dependence of the diameters of grids hole

Figure 9 shows the dependence of the diameter of screen grid hole. Other conditions are as follows: P_{abs} = 500 mW, V_0 = 1100 V, l = 0.8 mm, t_{sc} = 0.3 mm, t_{ac} = 0.3 mm, and d_{ac} = 1.8 mm. In this case, the calculated current density has become constant below d_{sc} = 3.2 mm. This is against the Child-Langmuir law, so that it would be inappropriate to include the diameter of the screen grid hole in effective gap distance l_e. In addition, the calculated current density has decreased at d_{sc} = 3.4 mm. We consider that the accelerator grid current has increased by the ion beam encountering the accelerator grid due to the increasing in the difference between hole diameter of the screen grid and that of the accelerator grid. Table 3 summarizes each current under the condition.

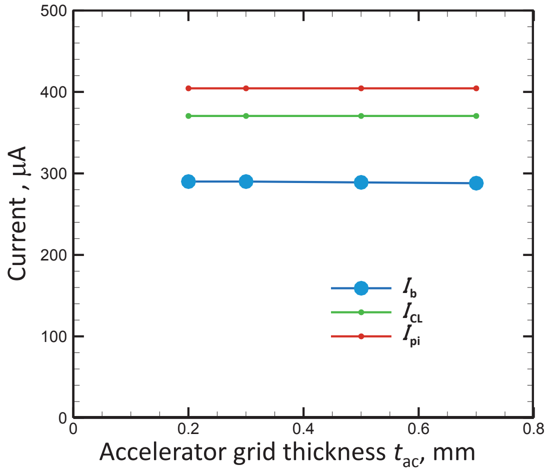

Figure 8. Dependence of the accelerator grid thickness.

Figures 10 and 11 show the dependence of the diameter of accelerator grid hole, where Fig. 10 is at d_{sc} = 3.2 mm and Fig. 11 is at d_{sc} = 3.4 mm. Other conditions are as follows: P_{abs} = 500 mW, V_0 = 1100 V, l = 0.8 mm, t_{sc} = 0.3 mm, and t_{ac} = 0.3 mm. There are turning points, such as d_{ac} = 1.8 mm for Fig. 10 and d_{ac} = 2.0 mm for Fig. 11. If the diameters of the accelerator grid hole are equal or greater than the values, the calculated current density has become constant. This tendency agrees with the Child-Langmuir law. On the other hand, if the diameters are smaller than the values, the calculated current density has decreased. We consider that it is due to the same reason as the dependence of the diameter of the screen grid hole. Tables 4 and 5 summarizes each current under the conditions, d_{sc} = 3.2 mm and d_{sc} = 3.4 mm, respectively.

In Figs. 9–11, the calculated current densities have decreased due to the increase in difference between hole diameters. Then, to find the relation between the diameters of screen and accelerator grids hole, we have investigated the ratio and the difference of hole diameters to the current density as shown in Figs. 12 and 13. It can be said that the difference between hole diameters is one of the useful parameters for ion beam extraction.

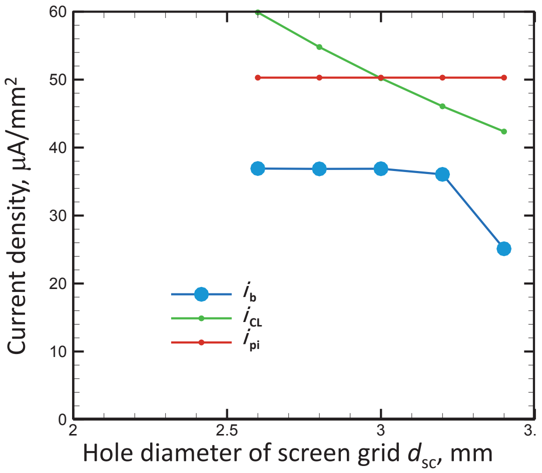

Figure 9. Dependence of the diameter of the screen grid hole.

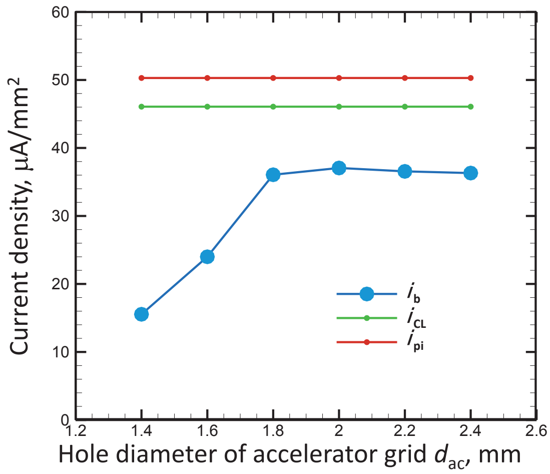

Figure 10. Dependence of the diameter of the accelerator grid hole (d_{sc} = 3.2 mm)

Table 3. Currents for dependence of the diameter of the screen grid hole.

d_{sc} (mm)	I_b (μA)	I_{sc} (μA)	I_{ac} (μA)
3.4	228	348	120
3.2	290	308	17.8
3.0	261	268	7.74
2.8	227	232	5.40
2.6	196	199	3.65

Table 4. Currents for dependence of the diameter of the accelerator grid hole (d_{sc} = 3.2 mm).

d_{ac} (mm)	I_b (μA)	I_{sc} (μA)	I_{ac} (μA)
1.4	125	311	186
1.6	193	308	116
1.8	290	308	17.80
2.0	298	307	8.77
2.2	294	301	6.86
2.4	292	297	5.21

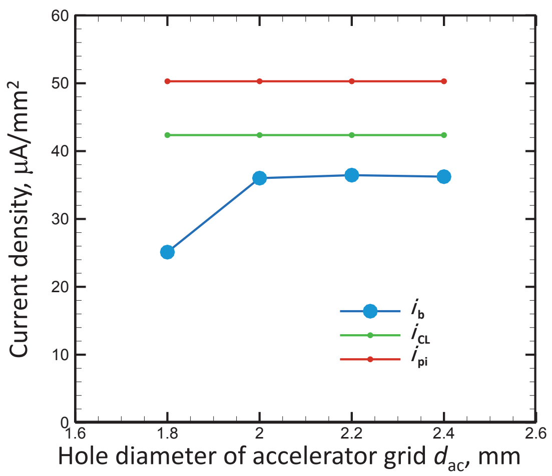

Figure 11. Dependence of the diameter of the accelerator grid hole (d_{sc} = 3.4 mm)

Table 5. Currents for dependence of the diameter of the accelerator grid hole (d_{sc} = 3.4 mm).

d_{ac} (mm)	I_b (μA)	I_{sc} (μA)	I_{ac} (μA)
1.8	228	348	120
2.0	327	344	17.3
2.2	331	341	10.0
2.4	329	337	7.92

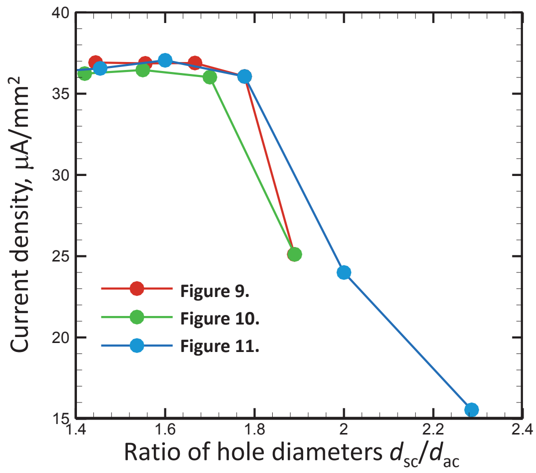

Figure 12. Dependence of the ratio of the hole diameters

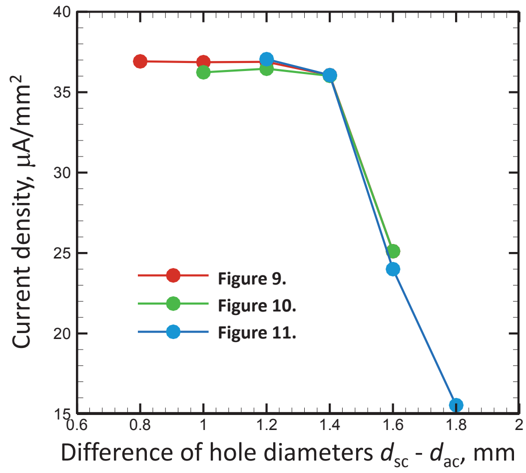

Figure 13. Dependence of the difference of the hole diameters

As described previously, the ion beam current depends on the gap distance between the screen and accelerator grids and the thickness of the screen grid, so that we have also investigated the dependence of the hole diameters difference with variations of the gap distance and the thickness of the screen grid. The results are shown in Figs. 14 and 15, where the former is fixed at t_{sc} = 0.3 mm and the latter is at l = 0.8 mm. Other conditions are as follows: P_{abs} = 500 mW, V_0 = 1100 V, and t_{ac} = 0.3 mm. As sown in Fig. 14, the turning point is 1.4 mm if the gap distance between the grids is smaller than 0.8 mm. In Fig. 15, likewise, the turning point is also 1.4 mm if the screen grid thickness is smaller than 0.5 mm. For ion thrusters, it is desirable to increase the diameter of screen grid hole and to reduce that of accelerator grid hole, so that the optimum value of the difference between the diameter of screen and accelerator grid hole is 1.4 mm.

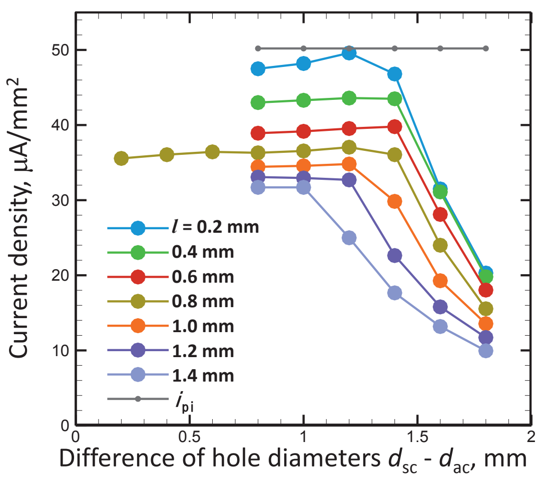

Figure 14. Dependence of the difference of the hole diameters in various *l* (t_{sc} = 0.3 mm)

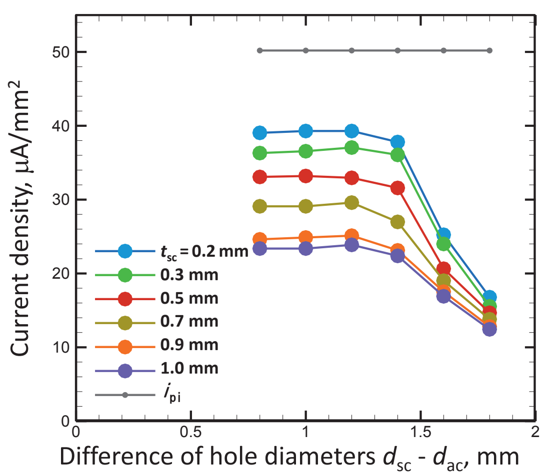

Figure 15. Dependence of the difference of the hole diameters in various t_{sc} (l = 0.8 mm)

IV. Conclusion

In this study, we have investigated the ion beam extraction mechanism by using PIC/MCC simulations. We have found that the increase in absorbed power (i.e., plasma density) is required to extract more ions from plasma region. We have also calculated under various conditions of grid structures. As a result, in relation to the previous effective gap distance between the grids, we have found that the ion beam current is affected by the gap distance of the grids and thickness of the screen grid, but is not affected by the diameter of the screen grid hole. In addition, we have also found that the optimum value of the difference between the diameter of the screen grid hole and that of the accelerator grid hole is 1.4 mm at an absorbed power of 500 mW, and that it is better to reduce both the gap distance between the grids and the thickness of the screen grid as small as possible. In future work, we will calculate under more various conditions, and experiment based on these results to examine the validity.

Acknowledgments

The computer simulation was performed on the KDK computer system at Research Institute for Sustainable Humanosphere, Kyoto University.

References

[1]Micci, M. M., and Ketsdever, A. D., *Micropropulsion for Small Spacecraft*, American Institute of Aeronautics and Astronautics, Reston, 2000.

[2]Koizumi, H., Komurasaki, K., Aoyama, J., and Yamaguchi, K., "Engineering Model of the Minature Ion Propulsion System for the Nano-satellite: HODOYOSHI-4," *Transactions of the Japan Society for Aeronautical and Space Sciences, Aerospace Technology Japan*, Vol. 12, No. ists29, 2014, pp. Tb_19-Tb_24.

[3]Patterson, M. J., Haag, T. W., Foster, J. E., Young, J. A., and Crofton M. W., "Development Status of High-Thrust Density Electrostatic Engines," *Proceedings of the 50th AIAA/ASME/SAE/ASEE Joint Propulsion Conference*, Cleveland, Ohio, USA, 2014, AIAA Paper No. 2014-3422.

[4]Patterson, M. J., Herman, D., Shastry, R., Van Noord, J., and Foster, J. E., "Annular-Geometry Ion Engine: Concept, Development Status, and Preliminary Performance," *Proceedings of the 48th AIAA/ASME/SAE/ASEE Joint Propulsion Conference & Exhibit*, Atlanta, Georgia, USA, 2012, AIAA Paper No. 2012-3798.

[5]Takao, Y., Sakamoto, M., Eriguchi, K., and Ono, K., "Investigation of Plasma Characteristics and Ion Beam Extraction for a Micro RF Ion Thruster," *Transactions of the Japan Society for Aeronautical and Space Sciences, Aerospace Technology Japan*, Vol. 12, No. ists29, 2014, pp. Pb_13-Pb_18.

[6]Hayashi, M., "Determination of electron-xenon total excitation cross-sections, from threshold to 100 eV, from experimental values of Townsend's a," *J. Phys. D*, Vol. 16, 1983, pp. 581-589.

[7]Heer, F. J. d., Jansen, R. H. J., and Kaay, W. v. d., "Total cross sections for electron scattering by Ne, Ar, Kr and Xe," *J. Phys. B,* Vol. 12, 1979, pp. 979-1002.

[8]Rapp, D. and Englander-Golden, P., "Total Cross Sections for Ionization and Attachment in Gases by Electron Impact. I. Positive Ionization," *J. Chem. Phys.,* Vol. 43, 1965 pp. 1464-1479.

[9]Boyd, I. D., "Modeling of the near field plume of a Hall thruster," *J. Appl. Phys.*, Vol. 95, 2004, pp. 4575-4584.

[10]Birdsall, C.K., and Langdon, A.B., *Plasma Physics via Computer Simulation*, IOP Publishing, Bristol, U. K., 1991.

[11]Vahedi, V., and Surendra, M., "A Monte Carlo collision model for he particle-in-cell method: applications to argon and oxygen discharges," *Computer Physics Communications*, Vol. 87, No. 1–2, 1995, pp. 179–198.

[12]Verboncoeur, J. P., "symmetric Spline Weighting for Charge and Current Density in Particle Simulation," *J. Comput. Phys.*, Vol. 174, No. 1, 2001, pp. 421–427.

[13]Verboncoeur, J. P., "Particle simulation of plasmas: review and advances," *Plasma Phys. Control. Fusion*, Vol. 47, No. 5A 2005, pp. A231–A260.

[14]Takao, Y., Kusaba, N., Eriguchi, K., and Ono, K., "Two-dimensional particle-in-cell Monte Carlo simulation of a miniature inductively coupled plasma source," *J. Appl. Phys*., Vol. 108, No. 9, 2010, pp. 093309–1~8.